BOEING SCIENTIFIC RESEARCH LABORATORIES DOCUMENT D1-82-0875

BOEING

SCIENTIFIC RESEARCH LABORATORIES

Some Diffraction Techniques for X-Ray Astronomy

Farrel W. Lytle

R. Graham Bingham

SOLID STATE PHYSICS LABORATORY JULY 1969

57

D1-82-0875

SOME DIFFRACTION TECHNIQUES FOR X-RAY ASTRONOMY

Farrel W. Lytle and R. Graham Bingham
Boeing Scientific Research Laboratories
Seattle, Washington 98124

July 1969

TABLE OF CONTENTS

1.0 ABSTRACT

Theories of x-ray diffraction applicable to x-ray astronomy techniques are developed. The preparation of crystals for maximum diffracted intensity is discussed and experimental measurements for LiF and graphite are given. The role of the "integrated reflection coefficient" in maximizing and calculating the effective gain of astronomical instruments is discussed. Two instruments, "The Confocal Paraboloid X-ray Lens" and "The Asymmetric Bragg Cosmic X-ray Polarimeter" are presented as examples and their performance estimated. A flight model of the Lens and a laboratory model of the Polarimeter have been constructed; details are given.

Definition of Symbols

n	order of diffraction
λ	wavelength
d	interplanar separation
θ	angle between incident ray and diffracting plane
θ_B	Bragg angle
ϵ	total number of photons recorded while tracing rocking curve
ω	angular velocity of crystal rotation
$I(\theta)$	intensity in diffracted beam at θ
I_o	total intensity in the incident beam
$R(\theta)$	$I(\theta)/I_o$
R	integrated reflection coefficient
R_m	R calculated from mosaic crystal theory (radians)
R_p	R calculated from perfect crystal theory (radians)
R^θ	R in radian units
R^E	R in energy units (keV)
R_a	R for asymmetric Bragg geometry
$\Delta\theta$	full width at half maximum of rocking curve
$\left(I(\theta)/I_o\right)_{max}$	ratio of diffracted to incident intensity at peak of rocking curve
E	x-ray energy in keV
r_e	classical electron radius; $e^2/mc^2 = 2.82 \times 10^{-13}$ cm
N	unit concentration of scattering units

F	structure factor
μ	total linear absorption coefficient
K_p	polarization factor for perfect crystal
K_m	polarization factor for mosaic crystal
ϕ	acute angle between crystal surface and diffracting plane
ψ	angle between diffracted beam and crystal surface
n'	x-ray index of refraction
Z	atomic number
A	atomic weight
m_H	mass of hydrogen atom
ρ	density
Δ	deviation from Bragg's law due to refraction
β	$\tan\phi/\tan\theta_B$

BLANK PAGE

2.0 INTRODUCTION

The low photon fluxes encountered in x-ray astronomy require development of large, passive collectors to concentrate celestial x-rays onto small sensors. In addition to the grazing incidence imaging systems proposed by Wolter[1] and developed by Giacconi et. al.[2], Kantor[3] has tested a concentrating arrangement of reflective glass slides and Lindquist and Webber[4] have constructed a parabolic array of NaCl crystals which focuses by Laue diffraction as x-rays pass through the crystals. We[5,6,7] have investigated devices utilizing Bragg diffraction from crystal surfaces and are encouraged by the properties inherent in crystal plane diffraction:

1. useful diffraction efficiency after correct crystal preparation;
2. monochromatic or broad band devices;
3. diffraction principle easily adapts to various collector geometries;
4. self-collimating with a small field of view (<0.5°);
5. sensitive to incident x-ray polarization.

The polarizing effect inherent in x-ray diffraction can be used for a sensitive and accurate measure of x-ray polarization. The theoretical and experimental basis for a practical device will be developed herein. This x-ray polarimeter should be compared with instruments using Thomson scattering from low Z materials developed by Novick[8] and by Sanin et. al.[9].

As part of an x-ray astronomy program a concentrating device using Bragg diffraction tailored for high altitude balloon x-ray observations has been designed and constructed. This instrument, "The Confocal Paraboloid

X-ray Lens", consists of nested aluminum support rings covered with a mosaic of LiF crystals each focusing by Bragg diffraction onto a small detector. The device promises high power in the diffracted beam with broad energy coverage and fine angular resolution.

3.0 DIFFRACTION THEORY

3.1 The Rocking Curve

In order to predict the utility of x-ray diffraction as a technique for x-ray astronomy (and ultimately to correct data to incident photon flux units) it is necessary to determine certain diffraction parameters. Diffraction maxima occur according to Bragg's law

$$n\lambda = 2d \sin\theta_B \qquad (1)$$

The diffraction profile is not infinitely sharp but spread through a small angle about θ_B. In Fig. 1a) a monochromatic, parallel x-ray beam is incident upon a plane crystal face large enough to intercept the entire beam. As the crystal is rotated at a uniform rate, ω , through θ_B the intensity of the diffracted beam $I(\theta)$ traces the "rocking curve" profile in Fig. 1b) with total number of photons under the curve equal to ϵ. If the fraction of the total incident beam diffracted at θ is given by

$$\frac{I(\theta)}{I_o} = R(\theta) \qquad (2)$$

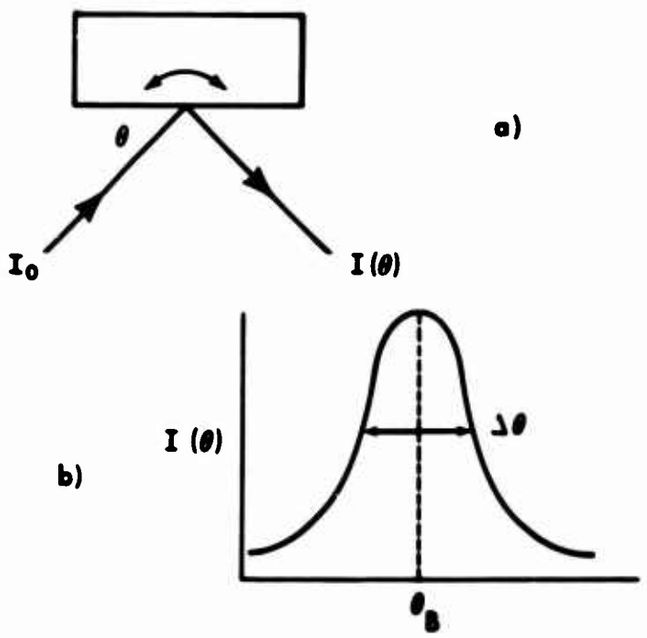

Fig. 1 a) Rocking Curve Experiment

b) Rocking Curve Profile

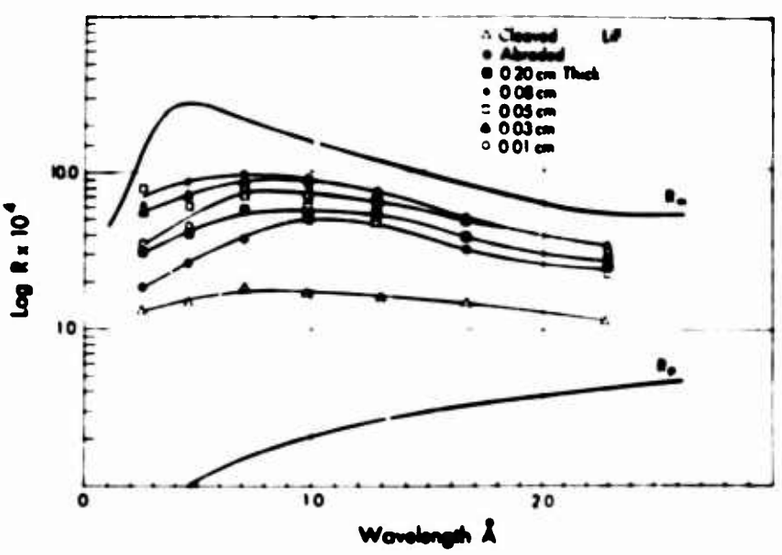

Fig. 2 Calculated ard absolute experimental values of the LiF (200) integrated reflection coefficient for unpolarized x-rays.

then

$$\frac{\varepsilon\omega}{I_o} = \int R(\theta)\, d\theta = R \text{ (radians)} \qquad (3)$$

R is defined[10] as the "integrated reflection coefficient", having the dimensions of radians, and is the angular range through which an equivalent amount of diffraction would occur at 100% efficiency. The full width at half maximum, $\Delta\theta$, is a convenient measure of diffractive dispersion. The product

$$\Delta\theta \left(\frac{I}{I_o}\right)_{max} \approx R \qquad (4)$$

is sometimes used to approximate R. The maximum diffraction efficiency, $(I/I_o)_{max}$, $\Delta\theta$, and R are of importance in x-ray astronomy since the maximum diffraction efficiency of any one wavelength is $(I/I_o)_{max}$ while $\Delta\theta$ (and the geometry of the device) determines the solid angle in which a celestial source must be found in order to be "seen" by the crystal planes. The rocking curve width, $\Delta\theta$, also determines the bandwidth of a device. In Fig. 1a) if the parallel x-rays incident upon the crystal contain a broad band of wavelengths then the <u>stationary</u> flat crystal segment at θ will diffract a band of wavelengths or energies

$$\left.\begin{aligned} \Delta\lambda &= \lambda \cot\theta\, \Delta\theta \\ \Delta E &= E \cot\theta\, \Delta\theta \end{aligned}\right\} \qquad (5)$$

which may be used to convert R^{θ} to R^{E}

$$R^{E} = R^{\theta}E \cot \theta \quad (\text{keV}) \tag{6}$$

This concept of a crystal segment selecting from an x-ray continuum and diffracting an appreciable range of x-ray energies proportional to its integrated reflection coefficient is fundamental to the development of useful astronomical instruments.

3.2 Integrated Reflection Coefficient

The theory of diffracted x-ray intensity describes two idealized limiting cases, (1) a perfect crystal lattice and (2) an ideal mosaic crystal consisting of many small domains with perfect internal lattice structure but slightly misoriented with respect to each other. The contributions of Darwin, Ewald, and von Laue on this and related subjects is summarized by James[11]. The integrated reflection coefficients of symmetric Bragg diffraction (diffracting plane parallel to crystal surface) for perfect and mosaic crystals are, respectively

$$R_p = \frac{8r_e N\lambda^2 F}{3\pi \sin 2\theta} \cdot \frac{1+ |\cos 2\theta|}{2} \quad \text{(radians)} \tag{7}$$

$$R_m = \frac{r_e^2 N^2 \lambda^3 F^2}{2\mu \sin 2\theta} \cdot \frac{1+ \cos^2 2\theta}{2} = \frac{Q}{2\mu} \quad \text{(radians)} \tag{8}$$

Graphs of R_m and R_p vs λ for LiF and graphite are shown in Figs 2 and 4. Tables I and II summarize the input parameters.

TABLE I Diffraction Parameters for LiF (200)

λ, Å	μ, cm^{-1}	$R_p \times 10^4$	$R_m \times 10^4$
0.1000	0.362	0.0206	4.23
0.2000	0.475	0.0432	13.5
0.2460	0.549	0.0532	17.8
0.3300	0.775	0.0713	24.4
0.4525	1.19	0.0968	28.6
0.5594	1.93	0.120	25.3
0.7093	3.54	0.151	21.8
1.0000	9.30	0.210	15.8
1.2818	18.0	0.263	12.7
1.6617	40.7	0.328	8.92
2.2897	102.0	0.408	5.68
3.0500	231.0	0.581	5.09
3.4500	324.0	1.06	7.02
3.6000	361.0	1.39	8.78
3.9500	478.0	4.26	25.3

$2d = 4.0267$ Å $\qquad \rho = 2.64$ gm cm^{-3}

$N = 1.531 \times 10^{22}$ cm^{-3} $\qquad F = 29.46$ at 22°C*

$$R_p = 5.38 \times 10^{10} \lambda^2 \left[\frac{1+|\cos 2\theta|}{\sin 2\theta}\right]$$

$$R_m = 4.00 \times 10^{21} \frac{\lambda^3}{\mu}\left[\frac{1+\cos^2 2\theta}{\sin 2\theta}\right]$$

μ determined from tables and equations in "International Tables for X-ray Crystallography", Vol. III, (Kynoch Press, Birmingham, England, 1962), p. 161.

* Atomic scattering factors for Li^+ and F^- from P.A. Doyle and P.S. Turner, Acta Cryst. A24, 390 (1968). Thermal parameters $B_{Li} = 0.90$ Å, $B_F = 0.63$Å from W. H. Zachariasen A24, 324 (1968).

TABLE II Diffraction Parameters for Graphite (002)

λ,Å	μ, cm^{-1}	$R_p \times 10^4$	$R_m \times 10^4$
0.100	.327	.0310	6.00
0.300	.468	.0930	11.30
0.500	.756	.1530	31.7
0.710	1.410	.217	68.5
1.295	6.32	.382	63.3
1.542	10.33	.461	41.3
1.937	20.0	.555	32.3
2.290	32.6	.661	26.6
2.750	55.8	.770	20.8
3.050	74.2	.833	18.4
3.600	121.0	.934	14.5
4.400	232.0	1.010	11.0
5.400	394.0	1.840	13.4
6.450	686.0	7.11	39.7

$2d = 6.708$ Å

$N = 2.821 \times 10^{22} cm^{-3}$

$$R_p = 4.59 \times 10^{10} \lambda^2 \left[\frac{1+|\cos 2\theta|}{\sin 2\theta}\right]$$

$$R_m = 2.91 \times 10^{21} \frac{\lambda^3}{\mu} \left[\frac{1+\cos^2 2\theta}{\sin 2\theta}\right]$$

$\rho = 2.21 g\ cm^{-3}$ (Compared to theoretical x-ray density of 2.25 g cm^{-3})

$F = 13.60$ at 22°C*

μ determined from tables and equations in "International Tables for X-ray Crystallography", Vol. III (Kynoch Press, Birmingham, England, 1962) p. 161.

* Atomic Scattering Factors for C from P.A. Doyle and P.S. Turner, Acta Cryst. A24, 390 (1968). Many thanks to Dr. J. Vierling for prepublication copy of calculations on graphite.

3.3 Extinction

The large difference in magnitude between the two equations is due to the relative coherence of the waves scattered by the two kinds of crystal. There is a $\pi/2$ change in phase with each diffraction event; thus, multiply diffracted waves in a crystal sufficiently perfect to maintain spatial coherence of the lattice and the incident and diffracted waves will form a dynamically coupled system transferring energy back and forth between two waves. (This phenomenon of "primary extinction" and the dynamic theory of diffraction has been much discussed; for example see Chandrasekhar[12], Lind, et. al.[13] and Batterman et.a.[14]). The effect of domain structure in a mosaic crystal is to make the diffracting volume small enough that primary extinction does not occur and to cause the scattering from separate domains to be incoherent. As x-rays penetrate a mosaic crystal two effects remove energy from the incident wave. (1) Each mosaic block subtracts a small amount and diverts it toward the diffracted direction, thus deeper lying blocks see a primary beam of lesser intensity. This is "secondary extinction" and has been discussed[11,12,13]. (2) Since the x-ray wave in the incident and diffracted direction is not coherent with the lattice, the ordinary linear absorption coefficient, μ, must apply. In the limit of very small domains so widely distributed in angle that the energy lost by absorption is much greater than by diffraction, the mosaic theory holds and $R_m = Q/2\mu$.

An understanding of extinction phenomena and the relationship to physical condition of the diffracting crystal is an essential part of optimizing diffraction techniques for x-ray astronomy, since real crystals fall in between the limiting cases and show both kinds of extinction. Nearly perfect crystals such as Si and Ge give results near R_p and, although $(I/I_o)_{max} \approx 90\%$, the rocking curve is very narrow - a few seconds of arc. The difficulty of fabrication techniques at this degree of accuracy as well as in the accompanying celestial pointing system make these crystals impractical at present for x-ray astronomy.

It is fortunate that more useful crystals are available and can be optimized for various diffraction-based devices through inducing a mosaic structure either by damaging a more perfect crystal or by progressively crystallizing polycrystalline material. LiF (200) and graphite (002) have high calculated integrated reflection coefficients which can be approached experimentally by these techniques.

3.4 Experimental Measurement of R

Lytle[15] compared cleaved and abrasively polished LiF at various wavelengths. Vierling et. al.[16] made a similar comparison and correlated Bragg diffraction intensity with dislocation density induced by a surface treatment. Since the abraded surface dislocation layer was only 50 microns thick the diffracted intensity was not as high for the more penetrating short wavelengths. However, a flexing treatment created dislocations throughout the crystal and increased the diffracted intensity at short

wavelengths. We have measured R from surface abraded LiF as a function of crystal thickness reasoning that R should increase with decreasing crystal thickness due to deeper penetration of dislocations because of less restraint by the base material. These results are shown in Fig. 2 as plots of R vs. λ and are actually higher than the flexed crystal of Vierling et. al.[16]. For the thinnest crystal, 0.01 cm, R decreases at the shorter wavelengths; however, crystals of thickness 0.03 - 0.08 cm diffract most intensely throughout the wavelength range investigated. The rocking curve width and (I/I_o) max are shown in Figs. 3a) and b). The test crystals were machined from pieces of the same crystal block with a milling machine "fly cutter" and used for diffraction measurements as machined. These results disprove the traditional rule that a diffraction crystal should be of the order of $1/\mu$ thick. For LiF $1/\mu$ at 0.2Å (62 KeV) is 2 cm and at 0.7Å (18 KeV) is 0.3 cm. In the interest of light weight with large areas of expensive crystal it is fortunate that crystal layers an order of magnitude thinner may be used.

"Highly oriented graphite" crystal[17] is prepared by annealing and hot pressing pyrolytic graphite. Gould et.al.[18] has shown its high diffraction efficiency and Vierling et.al.[16] have calculated R as a function of wavelength. Depending upon the degree of annealing and pressing, the rocking curve can vary from 2 to <0.5 degrees (see Fig. 6b). We have measured R vs λ for $\Delta\theta \approx 0.5°$ specimens and compare them with the calculated R_m in Fig. 4. $\Delta\theta$ and (I/I_o) max appear in Fig. 5a) and b). All crystals were 0.08 cm thick.

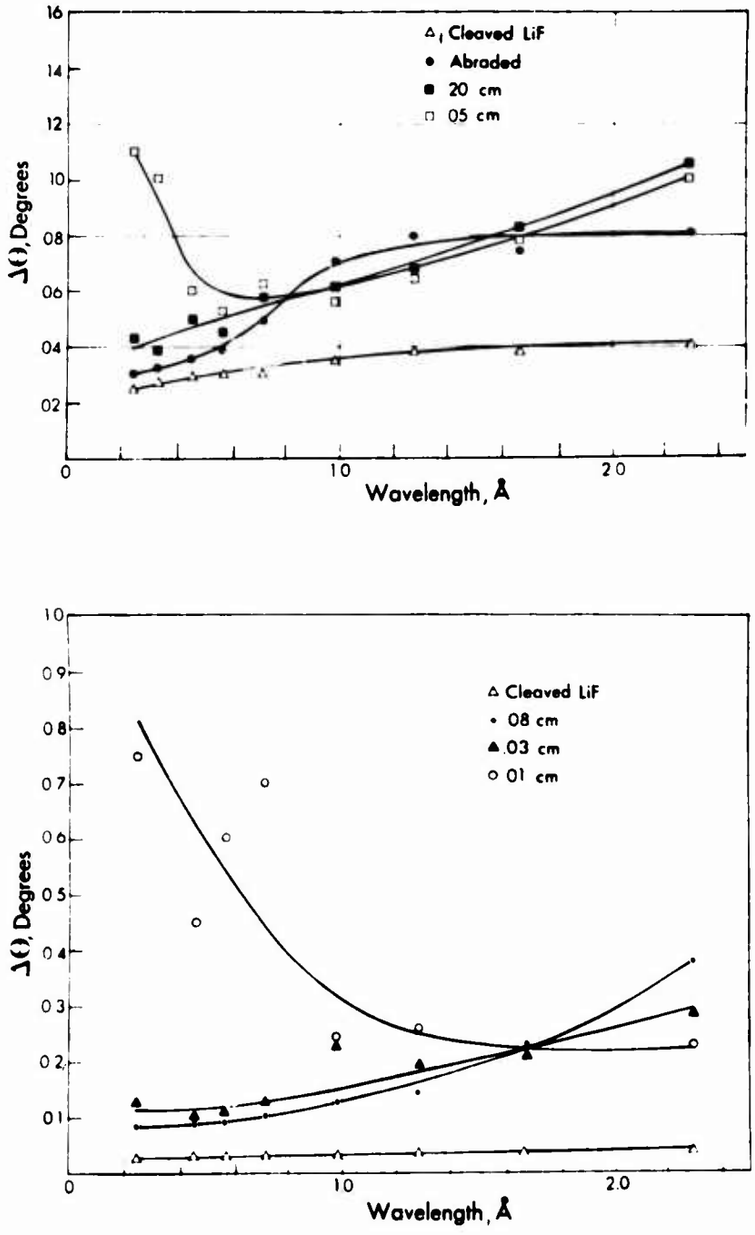

Fig. 3 a) Rocking curve width, $\Delta\theta$ for LiF (200)

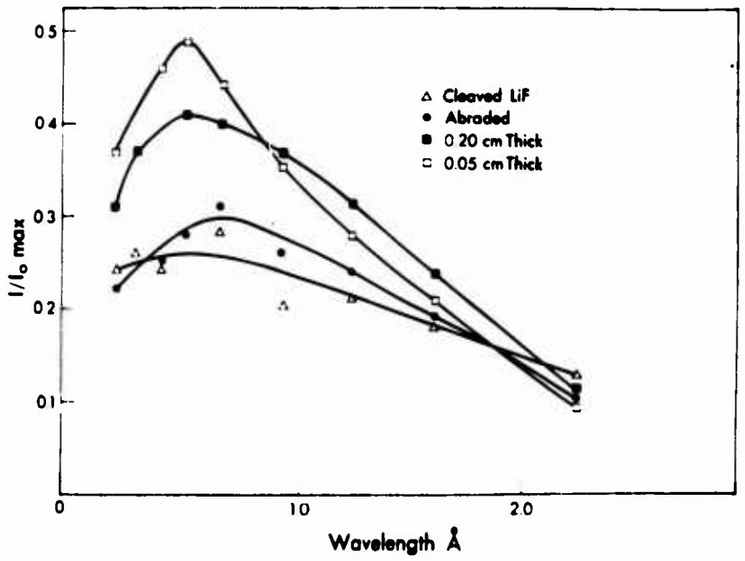

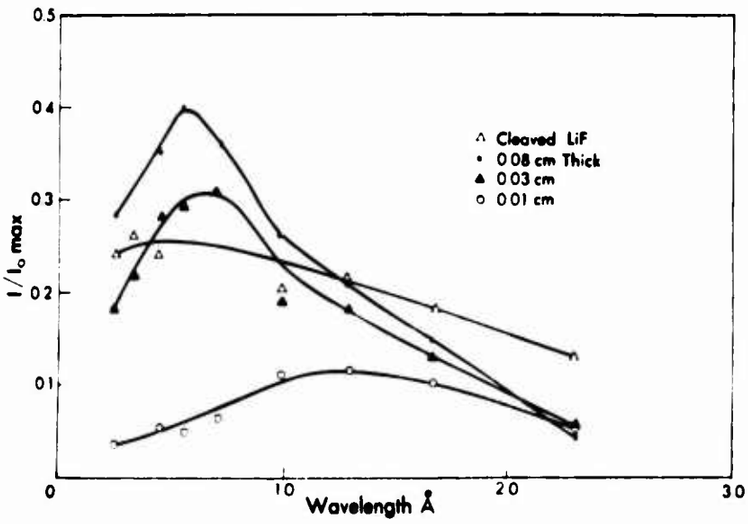

Fig. 3 b) Rocking curve intensity maximum, $\left(I/I_o\right)_{max}$ for LiF (200)

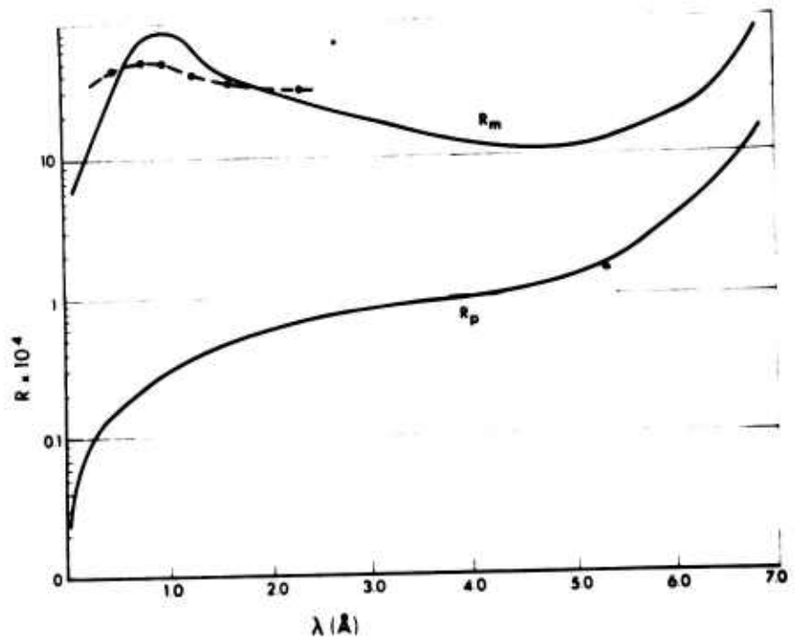

Fig. 4 Calculated and absolute experimental values of the "highly oriented graphite (002)" integrated reflection coefficient for unpolarized x-rays.

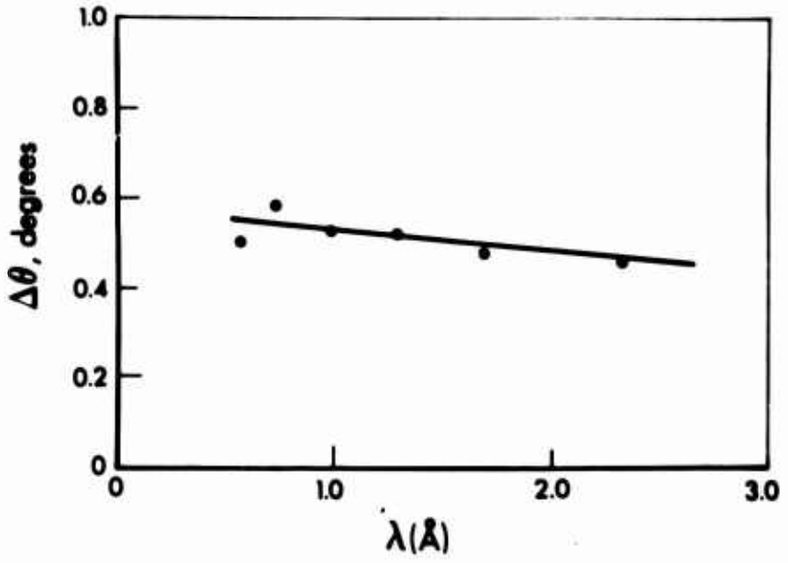

a)

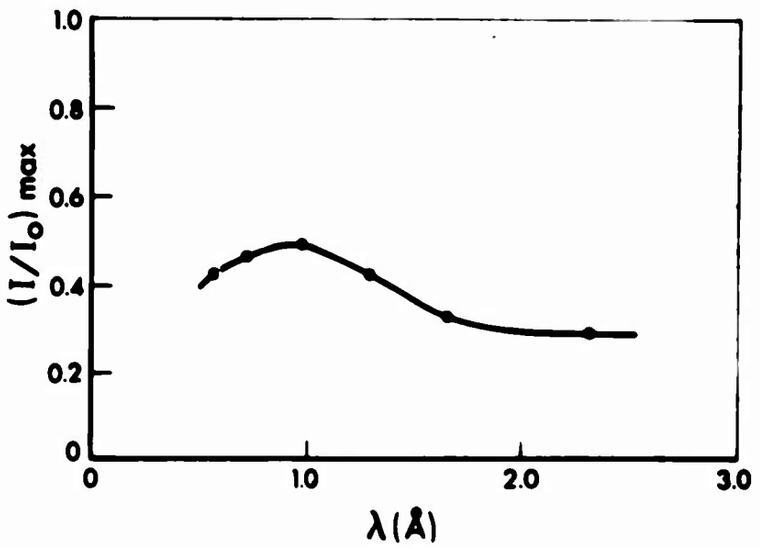

b)

Fig. 5 a) Rocking curve width, $\Delta\theta$, for graphite (002)

b) Rocking curve intensity maximum, $\left(I/I_o\right)_{max}$ for graphite (002).

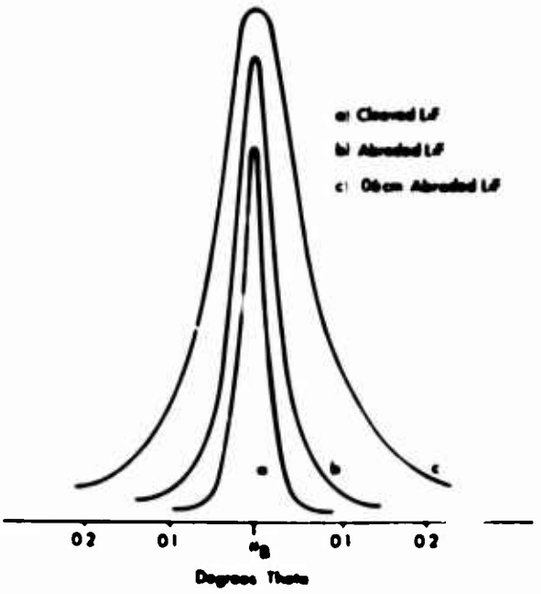

a)

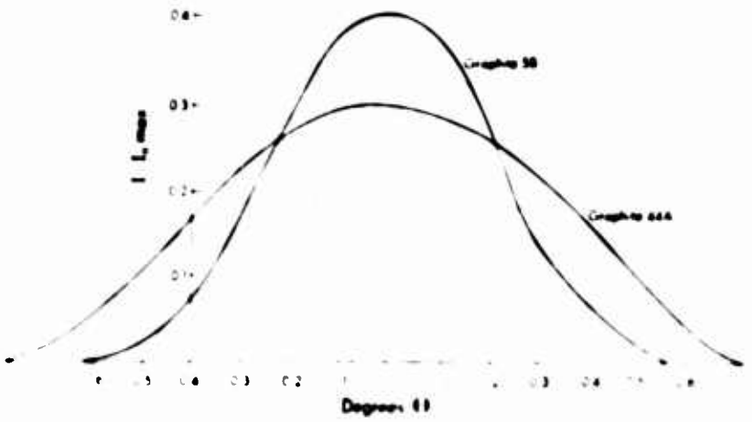

b)

Fig. 6 a) Experimental rocking curves for LiF (200) at 2.29Å.

b) Experimental rocking curves for graphite (002) at 2.29Å Sample 5B was used to measure R in Fig. 4.

3.5 Polarization Factor

The last term of equations 7 and 8 is the polarization factor for an unpolarized incident x-ray beam. The effect may be visualized by resolving the electric vectors of an incident x-ray beam into components perpendicular and parallel to the plane containing the incident and diffracted ray. The perpendicular component is diffracted without loss of intensity while the intensity of the parallel component is proportional to $|\cos 2\theta|$ for a perfect crystal or $\cos^2 2\theta$ for a mosaic crystal. Thus, the polarization factor for a perfect crystal, K_p, or a mosaic crystal, K_m

$$K_p = \frac{1}{2} \times 1 + \frac{1}{2} \times |\cos 2\theta| = \frac{1 + |\cos 2\theta|}{2} \qquad (9)$$

$$K_m = \frac{1}{2} \times 1 + \frac{1}{2} \times \cos^2 2\theta = \frac{1 + \cos^2 2\theta}{2} \qquad (10)$$

as used in equations (7) and (8). When $2\theta = 90°$ the parallel component becomes zero and the x-rays are plane polarized for either perfect or mosaic crystals. If the incident x-rays are already polarized to some degree, the relative magnitude of the two incident components would not be 1/2 and this could be detected as a deviation from the incident to diffracted intensity ratio of K_p or K_m. It is obvious that this effect can be used to measure the degree of polarization of incident x-rays if the diffracted intensity can be measured while rotating the diffraction plane around the axis of the incident ray. The polarizing cone, a device for doing this, is described in a later section.

The measurements of R for LiF and graphite were made using a double crystal spectrometer technique in which the first crystal, diffracting at θ_1, monochromatized and partially polarized the x-rays incident upon the test crystal at θ_2. Since the diffracted ray remained in the same plane and both crystals were mosaic, the total polarization factor is

$$K' = \frac{1}{2} \times 1 \times 1 + \frac{1}{2} \times \cos^2 2\theta_1 \times \cos^2 2\theta_2 \qquad (11)$$

The measured double crystal values were corrected to the case of an unpolarized incident beam for comparison to equation (8) by multiplying measured R by

$$\left(\frac{K_m}{K'} \right) K_m = \frac{1+\cos^2 2\theta_1}{1 + \cos^2 2\theta_1 \cos^2 2\theta_2} \cdot \frac{1+\cos^2 2\theta_2}{2} \qquad (12)$$

The polarization components for perfect and mosaic crystals, i.e. $|\cos 2\theta|$ and $\cos^2 2\theta$, introduce an indeterminacy into calculations for real crystals which may fit neither case. This has been investigated[19,20] and even used as a means of measuring extinction[23]. For practical estimates, calculations for abraded crystals of LiF or graphite should use the mosaic crystal formula. However, devices for accurate measurement of the degree of polarization of x-rays must be calibrated. Plane polarized x-rays for this purpose may be obtained by diffraction or scattering through 90° or by using the Borrmann[21,22] effect.

3.6 Asymmetric Bragg Geometry

When the surface of the crystal is cut at an angle, ϕ, to the diffracting planes, as in Fig. 7, an incident beam of width, W_o, is concentrated to width, W (or expanded if x-ray direction is reversed). This geometry was first described in detail by Renninger[24, 25] and investigated experimentally by Hirsch et. al.[26]. We have constructed a conical x-ray telescope[5,6] and proposed a cosmic x-ray polarimeter[7] based on this geometry. In a later section these instruments will be described in detail. The diffraction parameters are significantly changed from the symmetric Bragg case by the asymmetry and must be determined to design and evaluate the instruments.

The ordinary form of Bragg's law (equation 1) neglects the small effect of refraction at the crystal surface on the directions of the incident and diffracted rays. The index of refraction, n', of a substance for x-rays of wavelength, λ, such that λ is much shorter than any absorption edge[27] is

$$n' = 1-\delta = 1 - \frac{r_e \lambda^2 Z\rho}{2\pi m_H A} \tag{13}$$

$$\delta = 2.74 \times 10^{10} \lambda^2 \frac{Z\rho}{A} \tag{14}$$

And Bragg's law becomes

$$n\lambda \left(1 + \frac{\delta}{\sin^2 2\theta_B}\right) = 2d \sin \theta_B \tag{15}$$

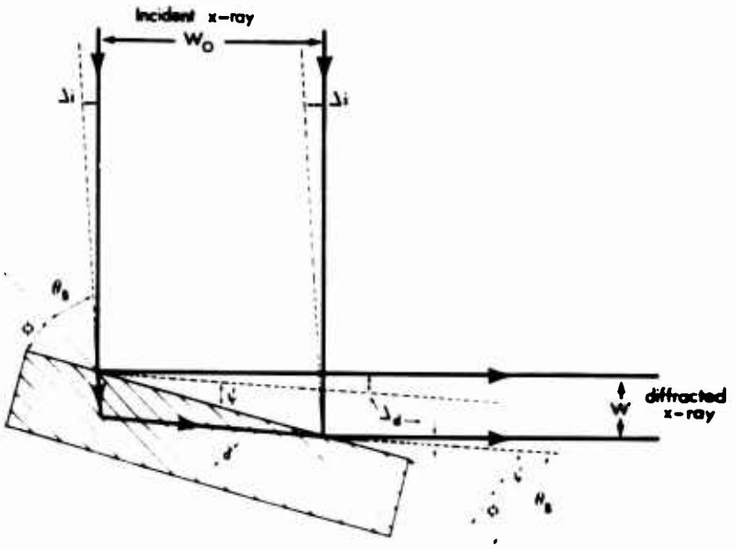

Fig. 7 Asymmetric Bragg diffraction from crystal planes inclined at an angle ϕ to the surface.

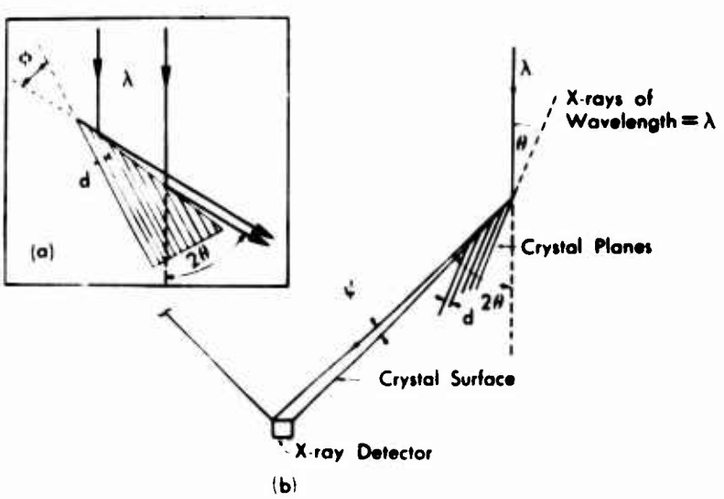

Fig. 8 Asymmetric Bragg Concentrating Device

a) A crystal segment from the surface

b) Cone of revolution around the x-ray detector

Since $\lambda^2 \approx 10^{-16}$ and $Z/A \approx 0.5$, δ is only a few parts per million and the effect is usually negligible. Because $n' < 1$ the angular deviation due to refraction is in the opposite direction from the optical case, i.e., the x-ray inside the crystal bends away from the surface normal. This is exaggerated in Fig. 7 where the dotted lines represent the directions predicted by the simple form of Bragg's law and the full line where diffraction actually occurs. The angle between these two directions is Δ; Δ_i and Δ_d for the incident and diffracted rays, respectively. For symmetric Bragg diffraction $\Delta = \Delta_i = \Delta_d$ and (in radians)

$$\Delta = \frac{\delta}{\sin\theta_B \cos\theta_B} \tag{16}$$

Renninger[25] has tabulated the diffraction parameters of interest in terms of the asymmetry index, β, where

$$\beta = \frac{\tan\phi}{\tan\theta_B} \tag{17}$$

$$\theta_B - |\phi| = \psi \tag{18}$$

Note that Renninger defines ϕ negative when the incident ray makes the larger angle with the crystal surface. Thus, in the sense of Fig. 7, ϕ is negative, and β approaches -1. The following discussion applies to this particular case.

The deviations from the Bragg angle due to refraction are

$$\Delta_i = \Delta \left(\frac{1}{1-\beta}\right) \tag{19}$$

$$\Delta_i + \Delta_d = 2\Delta \left(\frac{1}{1-\beta^2}\right) \tag{20}$$

Thus, the correction for the incident ray becomes one half the symmetric case while the correction for the diffracted ray may be significant when ψ becomes small.

The angular width of the diffraction pattern which we have characterized by the full width at half maximum, $\Delta\theta$ for symmetric diffraction, becomes

$$\Delta\theta_i = \Delta\theta \sqrt{\frac{1+\beta}{1-\beta}} \tag{21}$$

or for the diffracted ray

$$\Delta\theta_d = \Delta\theta \sqrt{\frac{1-\beta}{1+\beta}} \tag{22}$$

Thus, the angular width over which the Bragg condition is fulfilled becomes more narrow on the incident side while the emerging beam is diffractively dispersed over a greater angle.

The integrated reflection coefficient must also decrease with $\Delta\theta_i$ and

$$R_a = R_m(1+\beta) \tag{23}$$

for a mosaic crystal or for a perfect crystal

$$R_a' = R_p\sqrt{\frac{1+\beta}{1-\beta}} \tag{24}$$

It is evident that

$$\frac{R_a'}{R_p} > \frac{R_a}{R_m} \tag{25}$$

and once again the extinction problem introduces an uncertainty into calculations. For crystals such as LiF and graphite which are more nearly mosaic than perfect, equation (23) has not been experimentally verified, although the work of Gay, Hirsch, and Kellar[26] proved that $(I/I_o)_{max}$ remains high for small ψ; i.e. until $\psi \approx 1°$ for LiF. We shall use equation (23) with experimentally determined R from symmetric Bragg diffraction to calculate R_a. By equation (25) this should be a conservative estimate.

3.7 Asymmetric Bragg Concentrating Device

The concentrating device illustrated schematically in Fig. 8 consists of a cone covered on the inner surface with a mosaic of small asymmetric Bragg crystals oriented to diffract incident, parallel x-rays toward the apex where an x-ray sensor is located. Note that incident rays fulfilling the Bragg condition are mapped to definite points on the sensor. This is shown more clearly in Fig. 10. Since θ_B is constant the entire cone

selects from the incident x-ray flux a narrow band and diffracts it onto the x-ray sensor.

By definition R is the wavelength (or energy) interval over which an equivalent amount of radiation would be diffracted at 100% efficiency. Thus, the effective gain, g, is the product of the geometric concentration factor, G, and R_a (integrated reflection coefficient for the asymmetric Bragg case - equation 23)

$$g = G \times R_a \tag{26}$$

Since both G and R_a are functions of ψ and ϕ, equation (26) must be optimized. The geometric concentration factor is the ratio of the area of the cone opening to the detector area. Representing the cone and x-ray detector diameters by C and D,

$$G = \frac{C^2}{D^2} - 1 \tag{27}$$

It may be shown (after much geometry) that G is independent of all linear dimensions and given by

$$G = \left[\sin 4\psi \cot\phi - \cos 4\psi\right]^2 - 1 \tag{28}$$

where the detector area is unity.

The quantity

$$g/R = (1+\beta)G \tag{29}$$
$$= \left[1 - \frac{\tan(\theta-\psi)}{\tan\theta}\right] \left[(\sin 4\theta\cot\psi - \cos 4\theta)^2 - 1\right]$$

is plotted vs θ in Fig. 9 for 3 values of ψ. The maxima of the curves prove that the optimum concentrating device is achieved when $\theta = 18°$, although the gain is fairly constant (within a factor of two) from θ=8° to 30°. Plainly, ψ should be as small as possible. The available experimental data[26] prove that $\psi = 1.5°$ is a reasonable goal and will be used here for the purpose of performance predictions realizing that the optimum value of ψ must be determined by experiment. If R has been determined by integration of symmetric Bragg rocking curves as in Figs. 2 and 4, it must be converted to the asymmetric case and from radians to keV units which are compatible with differential photon flux units, $\Phi(E)$ (photons sec^{-1} keV^{-1} cm^{-2}), used in x-ray astronomy. By equations (1), (6), (23), and the conversion

$$\lambda \text{ (Å)} = \frac{12.398}{\text{keV}} \tag{30}$$

$$R^E = R^\theta \frac{12.4}{2d} \csc\theta\cot\theta \tag{31}$$

$$g = R^E G(1+\beta) \text{ (keV cm}^2\text{)} \tag{32}$$

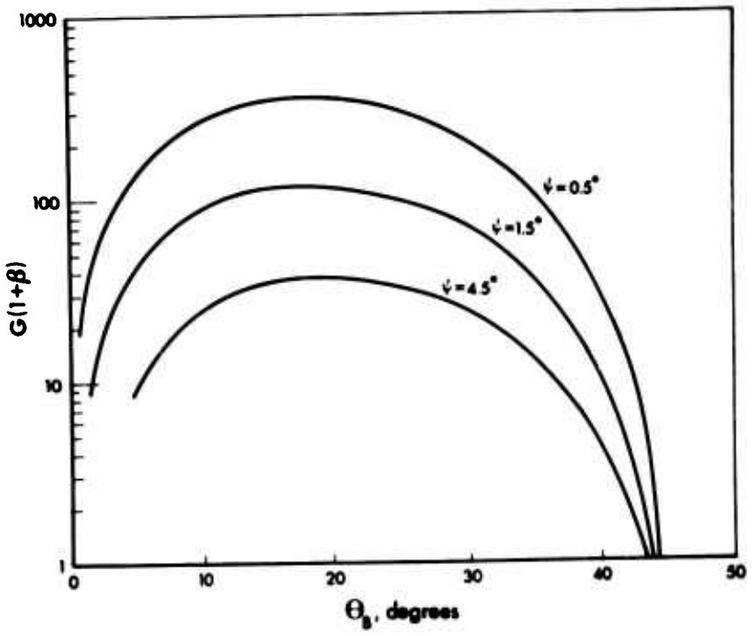

Fig. 9 Gain function of the asymmetric Bragg cone, $g/R = G(1+\beta)$

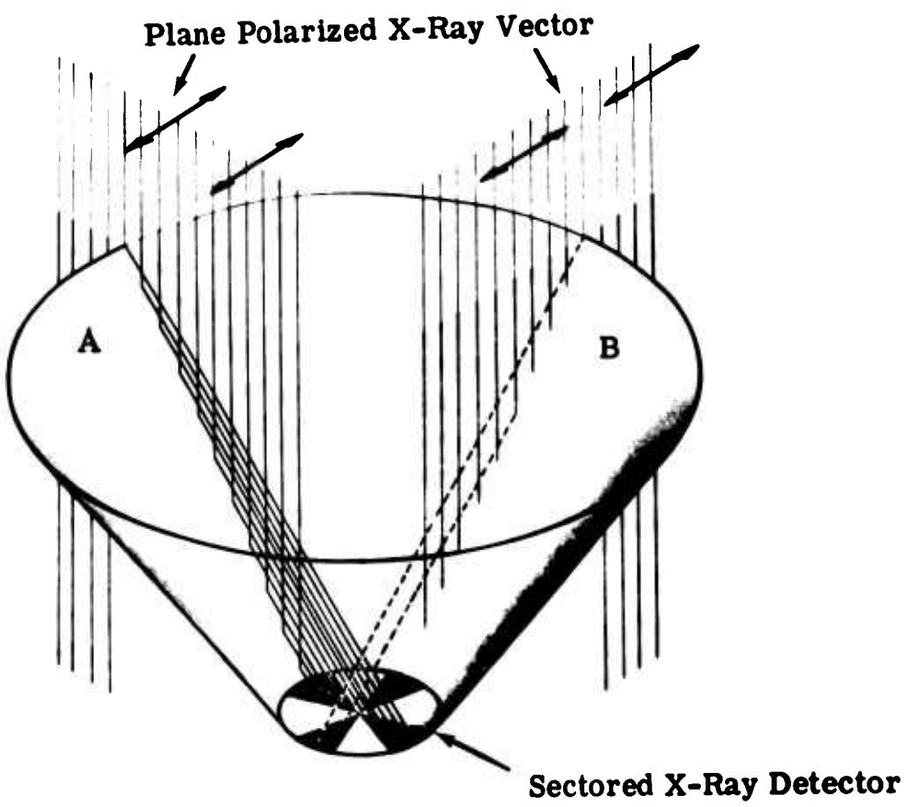

Fig. 10 Asymmetric Bragg Cosmic X-ray Polarizer

To use Fig. 9, read the value of g/R for the appropriate θ and ψ, multiply by R^E and g will be in units of keV cm^2. Then the photon rate at the detector

$$\text{photons sec}^{-1} = g \times \div(E) \times \text{detector area} \qquad (33)$$

The detector area enters into the product because in equation (28) the device is scaled to the detector as unity. A change in detector area linearly scales the entire device by equation (27). The physical dimensions of a cone optimized as a concentrator are given in Table III. Performance is estimated by a minimum detectable flux caculation in Table IV.

3.8 Asymmetric Bragg Cosmic X-ray Polarimeter

Optimization of the cone for use as a polarimeter must include the polarization factor inherent in x-ray diffraction. In Fig. 10 the cone-to-detector mapping of selected rays is shown. For incident plane-polarized x-rays with the polarization vector as illustrated, the diffracted intensity from mosaic crystals on the two orthogonal sector pairs will be in the ratio of $1:\cos^2 2\theta_B$ from A and B, respectively. The degree of polarization is determined by summing the counting rate in opposite sectors and measuring the differences between orthogonal sector pairs.

Let c_i be the counting rate in the i^{th} sector pair where $i = 4$ corresponds to the sector diffracting at maximum intensity and $i = 3,2,1$ to

TABLE III Optimized Cone Parameters with 5 cm^2 Detector (ψ= 1.5°)

	Concentrator		Polarimeter	
	LiF	graphite	LiF	graphite
2d, Å	4.0267	6.69	4.0267	6.69
θ, degrees	18	18	29	29
λ, Å	1.24	2.07	1.95	3.24
energy, keV	10.0	5.99	6.36	3.83
R^{θ}, radians	7.7×10^{-4}	32×10^{-4}	4.1×10^{-4}	20×10^{-4}
R^{E}, keV	2.4×10^{-2}	5.9×10^{-2}	0.47×10^{-2}	1.4×10^{-2}
g/R	113	113	74	74
g, $keVcm^2$	2.7	6.7	0.33	1.05
diameter, cm	92	92	86	86
area of, cm^2 opening	6440	6400	5850	5850
Total height, cm including detector	70	70	40	40

TABLE IV Minimum Detectable Flux, $\Delta I(E)_{min}$ for Graphite Cone Concentrator at Satellite Altitude

---

Si(Li) detector with area $A_D = 5\ cm^2$ and bandwidth $\Delta E_D = 1$ keV

observing time $t = 1000$ sec.

satellite altitude ~ 300 Km

graphite cone $g = 6.7$ for 6 keV photons

width of rocking curve $\theta_i = 0.1°$

field of view of cone $\Omega_c = 10^{-5}$ steradian

field of view of detector alone $\Omega_D = 10^{-1}$ steradian

Inherent detector background $IB = 4 \times 10^{-4}$ photon cm^{-2} sec^{-1} keV^{-1}

Isotropic flux $IS = 4 \times 10^{-1}$ photon cm^{-2} sec^{-1} keV^{-1} $steradian^{-1}$

At the 3σ (99.7% confidence level)

$$\Delta I(E)_{min} = 3\sqrt{\text{Total background}/g(A_D t)}^{\frac{1}{2}}$$

$$= 3\left\{ IB \times \Delta E_D + \left[IS \right] \left[g\Omega_c + \Delta E_D \Omega_D \right] \right\}^{\frac{1}{2}} \Big/ g(A_D t)^{\frac{1}{2}}$$

$$\Delta I(E)_{min} = 1.3 \times 10^{-3} \text{ photon } cm^{-2} sec^{-1} keV^{-1}$$

$$2 \times 10^{-4} \text{ the intensity of Sco XR-1(6keV)}^*$$

---

*Gould, R.J. Am. J. Phys. 35, 376 (1967).

decreasing magnitudes of detected flux. The parameter, P , measures the degree of linear polarization, where

$$P = \frac{I_A - I_B}{I_A + I_B} \tag{34}$$

and I_A and I_B are the incident x-ray intensities parallel and perpendicular to the direction of polarization (if any). Integration over the finite angular width of the detecting sectors shows that

$$P = K \frac{\left[(C_4-C_2)^2 + (C_1-C_3)^2\right]^{1/2}}{C_1+C_2+C_3+C_4 - 4N} \tag{35}$$

where N is the x-ray background per sector pair, and is assumed to be unpolarized. The constant K is the reciprocal value of apparent polarization measured for a given polarimeter illuminated by a fully polarized incident beam, and should lie in the range determined by the limit of perfect and mosaic crystals

$$\frac{\pi(1+|\cos 2\theta|)}{\sqrt{2}(1-|\cos 2\theta|)} \geq K \geq \frac{\pi(1+\cos^2 2\theta)}{\sqrt{2}\sin^2 2\theta} \tag{36}$$

A Gaussian error analysis adopting a Poisson statistic shows the standard deviation of P is given by

$$\sigma_P = K\left[2\sum_{i=1}^{4} C_i\right]^{-1/2}, \tag{37}$$

if $N = C_1$.

To obtain the optimum polarimeter we wish to minimize σ_p. Ignoring the spectral shape (continuum) of any incident (celestial) x-ray flux one can minimize σ_p by maximizing $\left| \sum_{i=1}^{4} C_i \right|$ and minimizing $K(\theta)$ using equation (37). Thus, for the optimum polarimeter $\theta = 29°$. Specific instruments for stellar x-ray polarimetry must be tailored to the spectral hardness of the class of celestial objects being observed. The parameters of a $\theta=29°$ polarimeter are given in Table III and performance on a celestial source estimated in Table V. This design for a 5 cm^2 detector can be scaled to either smaller or larger detectors with correspondingly decreased or increased sensitivity.

3.9 Cone Ray Tracing Studies

The response to off-axis x-ray sources (hence, the requisite celestial pointing accuracy) was investigated by a computer ray tracing program. A simulated parallel x-ray beam distributed over the area of the cone opening in a uniform-random manner was made to fall on the crystal surface and undergo asymmetric Bragg diffraction. The point-to-point mapping from the cone to the detector was investigated for paraxial rays and various angles off axis. These results are shown in Fig. 11 where a), b), and c) represent the ray diagram onto a single unit detector in a cone which would be used as a simple concentrating device. Approximately 13% and 20% of the photons would miss the detector in cases b) and c) respectively. Thus, a pointing system accuracy of 0.25° appears reasonable. The more stringent mapping required for a sectored detector is shown in Fig. 11d), e), and f). In

Table V Polarimeter Precision for Crab Nebula

ψ = 29°	g(cm^2keV)	E(keV)	K	$\dot{}(E)_{Crab}$ ($cm^{-2}sec^{-1}keV^{-1}$)*	Total Photons (1000 secs)	σ_p(%)
Lithium Fluoride	0.33	6.4	3.9	0.17	280	16
Graphite	1.05	3.8	3.9	0.5	2700	5

detector area = 5 cm^2, ψ = 1.5°, Mosaic crystal

*Boldt et al, Ap. J., 156, 427, 1969

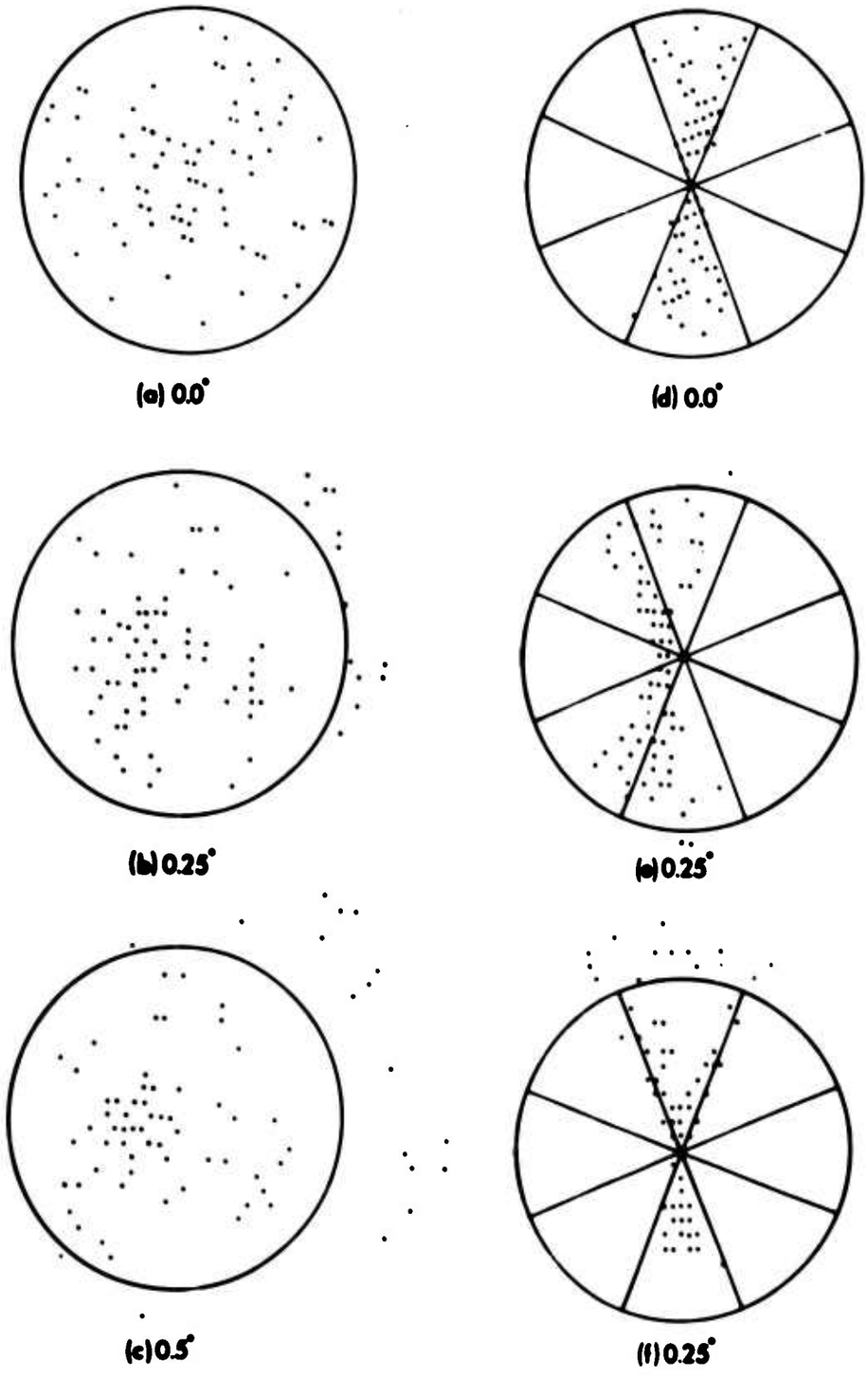

Fig. 11 Computer Simulated Cone-to-detector mapping for paraxial and off-axis x-rays

this case a 0.25° error seriously degrades the polarization information; probably a pointing system with 0.1° accuracy would be required, which is well within presently existing altitude control systems of rocket/satellite instrumentation.

4.0 ASYMMETRIC BRAGG LiF CONE

To gain experience in fabrication techniques and to demonstrate the concentrating properties of this geometry a laboratory version (shown in Fig. 12) has been constructed tuned to λ = .7093 or 17.5 keV (the Mo $K\alpha_1$ line). The cone had a diameter C = 15 cm, a detector diameter D = 2 cm and utilized LiF as the diffracting crystal. These unoptimized dimensions gave ψ = 4.5° and θ_B = 10.15°. After machining the cone from solid aluminum at the cone angle = $4\theta_B - 2\psi$, the entire inner surface was machined into 0.6 cm deep grooves cut at an angle to accept the mosaic of cleaved 0.6 cm LiF cubes. The cubes were cemented into the grooves (thus covering the surface) and then the cone angle was re-machined into the LiF. The final surface was smoothed with abrasive paper, etched 1 min. in conc. HF, and 10 min. in 5% NH_4OH aqueous solution to remove surface debris. The finished surface is shown in the photograph.

It was not possible to measure the gain of the entire cone because a large area collimated x-ray beam was not available. However, the focusing properties were demonstrated as in Fig. 13 where x-rays from a Mo target x-ray tube were collimated to $\approx 2°$ divergence by a distance of 2.1m. The photograph (Fig. 12) shows the diffracted beam converging toward the planned 2 cm diameter focus at distances of 4 cm, 2 cm, and 0 cm from the

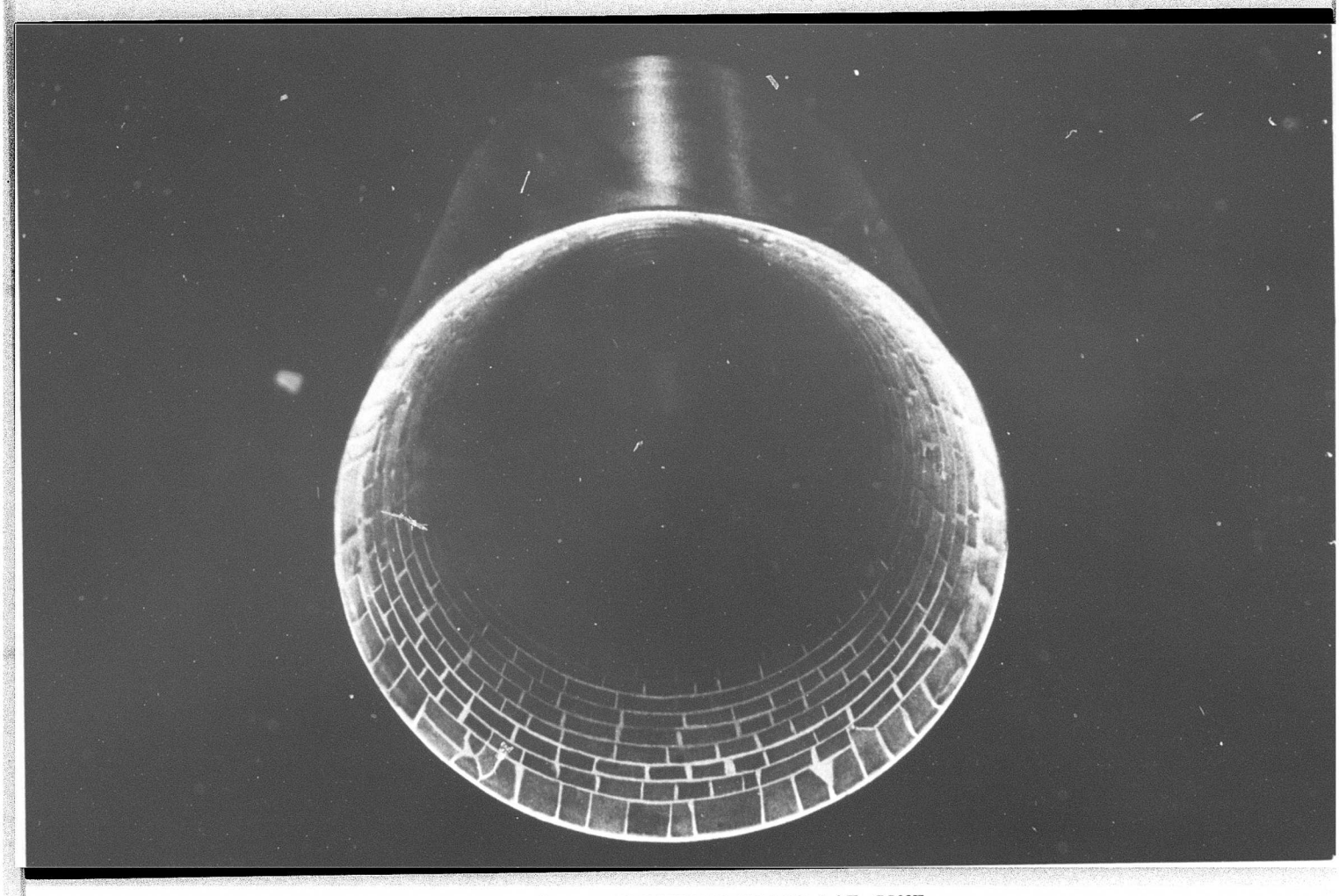

Fig. 12 a) ASYMMETRIC BRAGG LiF CONE

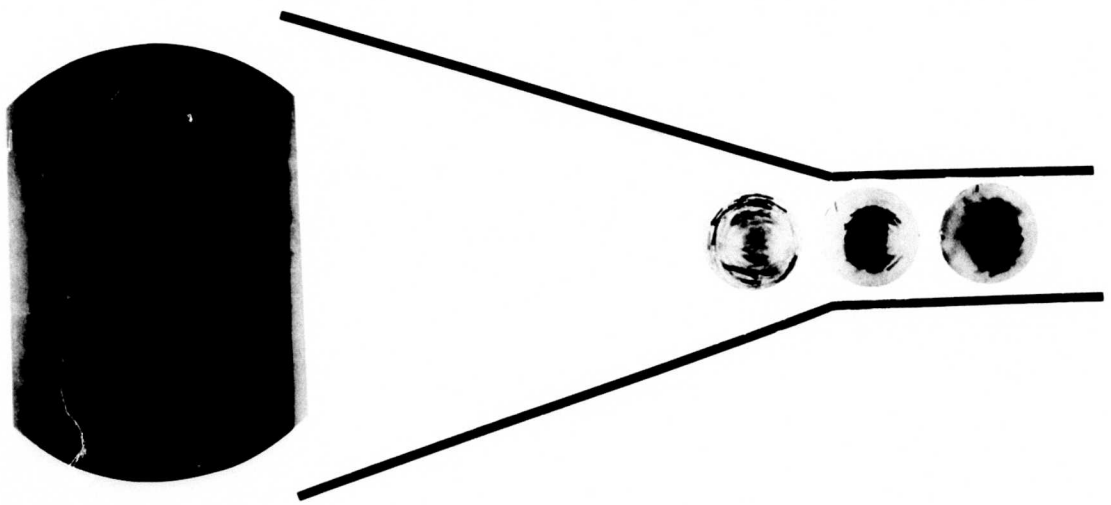

b) DIFFRACTED BEAM CONVERGING TO A FOCUS

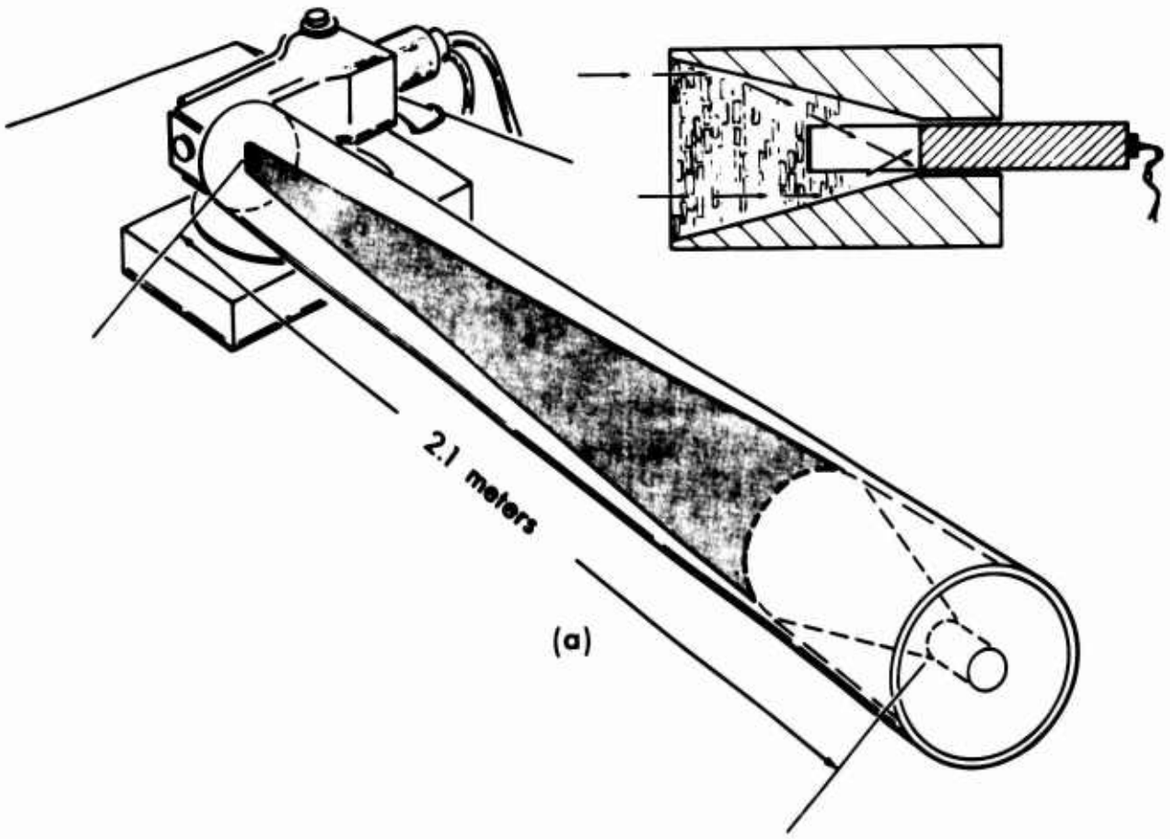

Fig. 13 X-ray test arrangement

focal plane. Because of the 2° divergence of the beam and the narrow rocking curve (0.1°) of the LiF only the innermost crystals were diffracting with full intensity. When a scintillation counter was inserted into the detector position a significant enhancement was observed compared to the unconcentrated incident beam, although an absolute determination of gain was not possible.

5.0 CONFOCAL PARABOLOID X-RAY LENS

As part of an x-ray astronomy program we have designed and constructed an x-ray concentrating device utilizing Bragg diffraction tailored for high altitude balloon x-ray observations. The geometry was chosen to provide:

a) high power in the diffracted beam

b) broad energy coverage

c) fine angular resolution

The system consists of nested aluminum support rings covered with a fine mosaic of LiF crystals; after affixing to the rings, the crystal surface on each ring was machined into a paraboloidal surface designed to concentrate (by symmetric Bragg diffraction) a parallel beam of x-rays onto a small (5 cm^2) detector.

The device, sketched in Fig. 14, shows that the angle of incidence, θ_B, is gradually and continuously increased as photons are diffracted from annuli of increasing diameter. Thus, low energy x-rays are diffracted by the larger annuli, and high energies by the smaller annuli. Since the change in θ_B is nearly continuous, the lens will concentrate a beam of x-rays over the range from 18 to 100 KeV. Fig. 15 is a photograph of the final lens assembly.

The geometry of the lens allows unobstructed passage of incident and diffracted rays while having maximum projected sensing area and self-collimation to almost eliminate off-axis x-rays. The overall diameter is 50" (inches) with not less than 0.4" between adjacent annuli. Each of the 19 annuli consists of 0.025" thick LiF crystals epoxied onto a 0.1" aluminum support ring with a height of 10.0". The distance from the

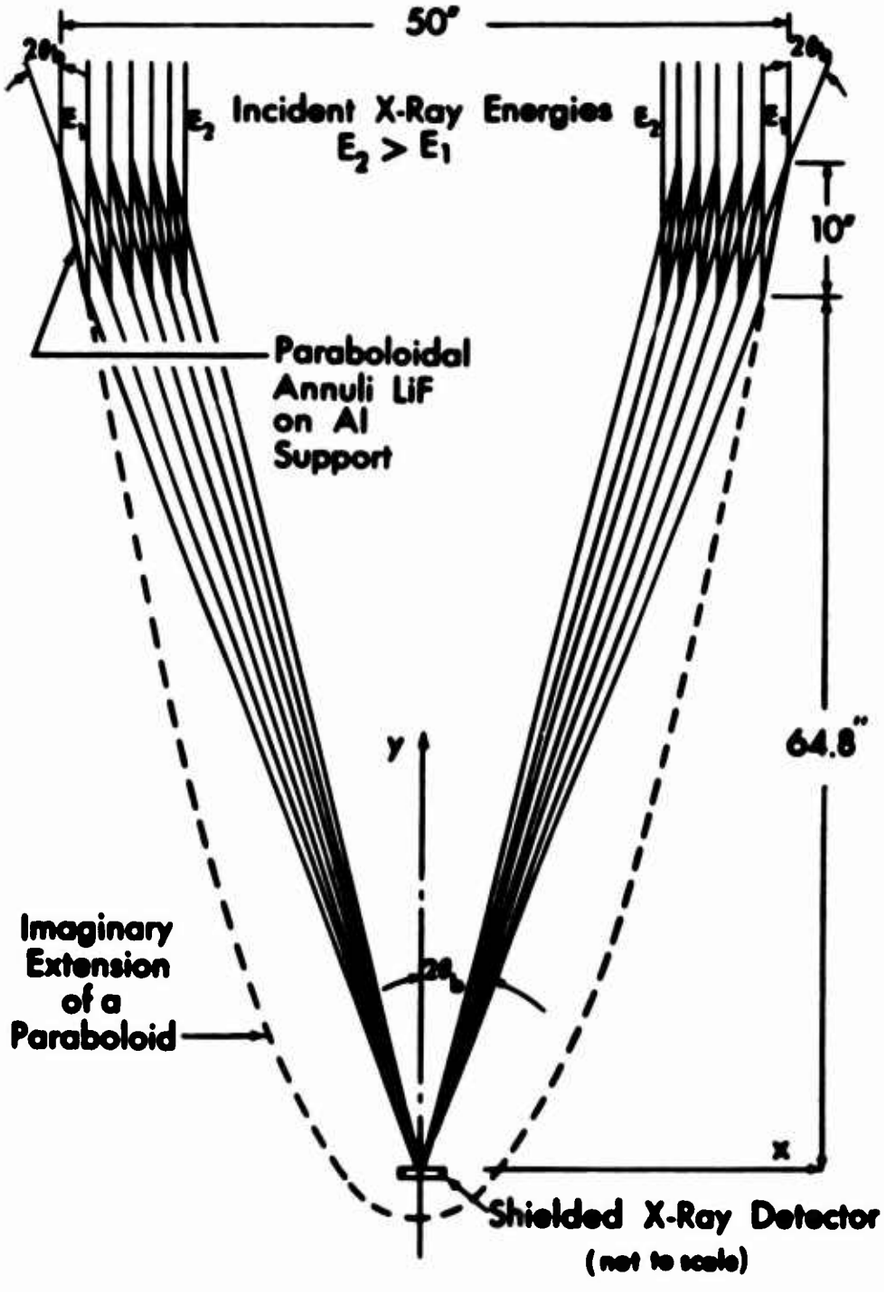

Fig. 14 Concentrating principle of x-ray lens

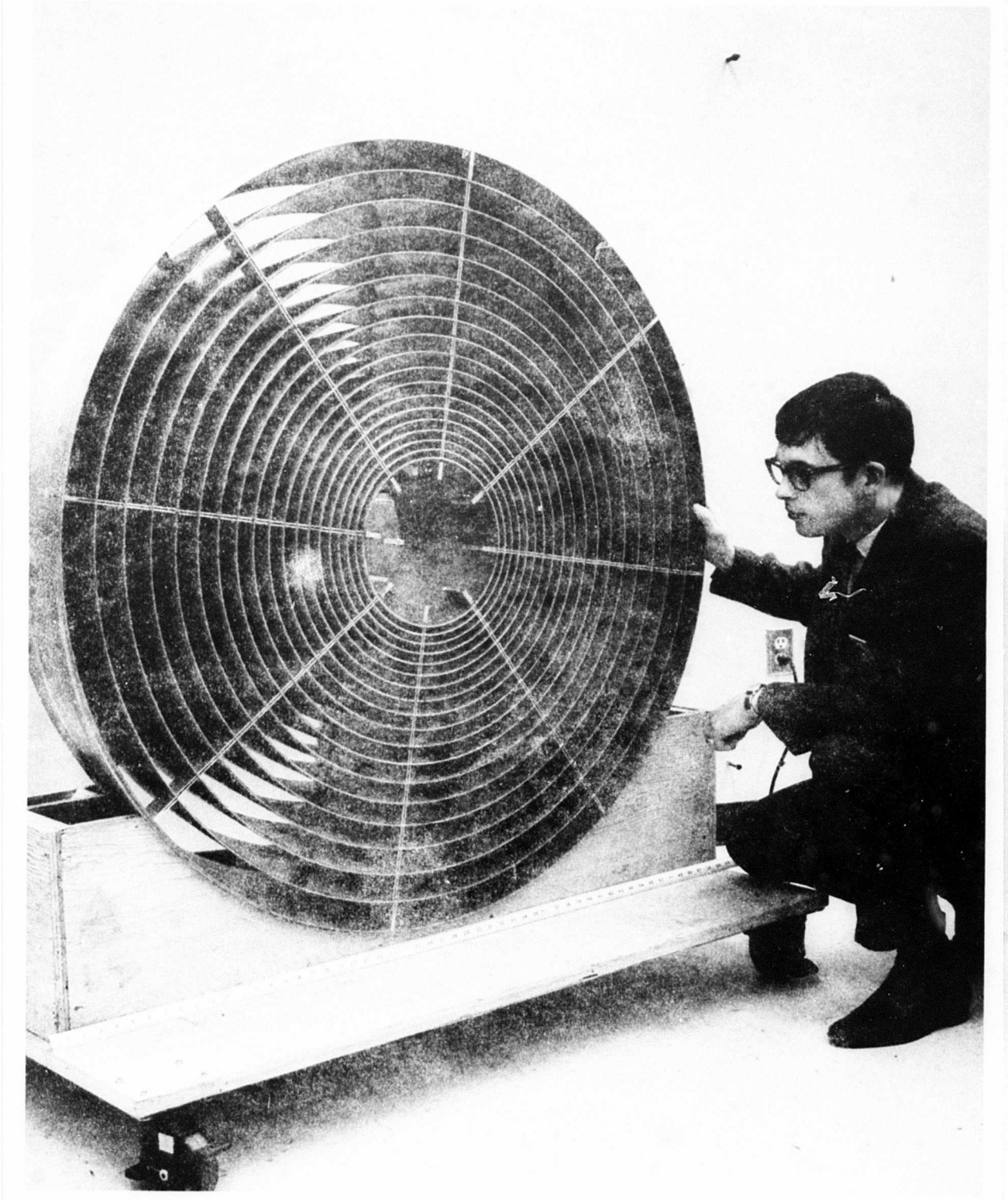

Fig. 15 CONFOCAL PARABOLOID X-RAY LENS

bottom of all annuli to the focal plane is 64.8". Paraboloidal sections provide first order diffraction from 18 to 87 keV, which is consistent with expected extraterrestrial x-ray spectra after attenuation through 3g cm^{-2} residual atmosphere. Second order diffraction extends the range to 100 KeV with higher orders being of negligible intensity.

Of prime importance in estimating the effectiveness of this x-ray lens is a knowledge of the effective projected sensing area as a function of energy, represented by the differential quantity dA(E). Using the cartesian coordinates shown in Figure 14, each parabolic cross section may be represented by the equations

$$x^2 = k^2+2ky \tag{38}$$

and

$$x = k \cot\theta_B \tag{39}$$

where k is a constant for a given annulus. Values of k for the 19 actual paraboloids are listed in Table VI. The value dA(E) is obtained by considering a monoenergetic, paraxial beam of x-rays with intensity I_0 impinging onto the lens, and integrating over the range of incident angles θ this beam will exhibit diffraction. That is,

$$dA(E) = \int_{\theta}^{\infty} \frac{dA}{d\theta} \cdot \frac{I(\theta)}{I} \cdot d\theta \tag{40}$$

TABLE VI Values of Parameter k

	Inches
k_1	4.029
k_2	3.450
k_3	2.950
k_4	2.521
k_5	2.151
k_6	1.833
k_7	1.560
k_8	1.325
k_9	1.124
k_{10}	0.951
k_{11}	0.804
k_{12}	0.677
k_{13}	0.570
k_{14}	0.478
k_{15}	0.399
k_{16}	0.333
k_{17}	0.276
k_{18}	0.228
k_{19}	0.188

k_1 corresponds to the largest annuli;

k_{19} to the smallest

where $I(\theta)$ is the diffracted intensity at angle θ, and

$$\frac{dA}{d\theta} = \frac{dA}{dx} \cdot \frac{dx}{d\theta} = 2\pi k^2 \frac{\cos \theta_B}{\sin^3 \theta_B} \approx \frac{2\pi k^2}{\sin^3 \theta_B} \quad (\theta_B \leq 9°) \tag{41}$$

Consideration of experimentally measured diffraction patterns of LiF in Fig. 3a) shows the *useful* range of integration is 0.1 to 0.2°. Thus $\frac{dA}{d\theta}$ can be sensibly considered a constant for each integration of equation (40) at a particular energy (E). Therefore,

$$dA(E) = \frac{2\pi k^2}{\sin^3 \theta_B} \int_0^\infty \frac{I(\theta)}{I_o} d\theta = \frac{2\pi k^2 R}{\sin^3 \theta_B} \tag{42}$$

where R is the integrated reflection coefficient, defined in equations (2) and (3).

From the Bragg equation and equation (42), we obtain for LiF ($2d = 4.03$Å)

$$dA(E) = \frac{2\pi k^2 E^3}{(3.1 \times n)^3} R^\theta \tag{43}$$

where E is in keV and R^θ must be specified for a given order of diffraction and photon energy and in radian units.

In Fig. 2, R has been experimentally determined for the particular LiF thickness and surface preparation used in the construction of the x-ray lens. The results show R^θ is essentially constant over the

designed range of energies (18 to 100 keV) and has the values

$$R(n = 1) = 7 \times 10^{-4} \text{ radians}$$
$$R(n = 2) = 1 \times 10^{-4} \text{ radians}$$

Computation using equation (43) yields the differential effective projected area of the lens as a function of energy. Figure 16 shows dA(E) smoothed for clarity; the curve is deliberately chosen to be 10% conservative thus allowing for any constructural imperfections.

5.1 Angular Resolution

A singular characteristic of the x-ray lens system is its ability to measure angular locations of discrete celestial objects with a precision of 2 to 3 arc minutes. This estimate of angular resolution is based upon the following considerations of the total field of view.

Three factors govern the field of view. Listed in decreasing order of importance, these factors are:

a) The aluminum supporting rings of the diffracting LiF are essentially opaque for x-rays arriving at off-axis angles > 0.6°. The degree of opaqueness is slightly energy dependent.

b) The finite size of x-ray detectors to be placed in the focal plane further restricts the acceptance of non-paraxial x-rays.

c) Of lesser but not negligible consideration is the finite width of the "rocking curve" (0.1° to 0.2°) of LiF. Thus we estimate the field of view to be $\leq 0.5°$; this is dependent upon the accuracy

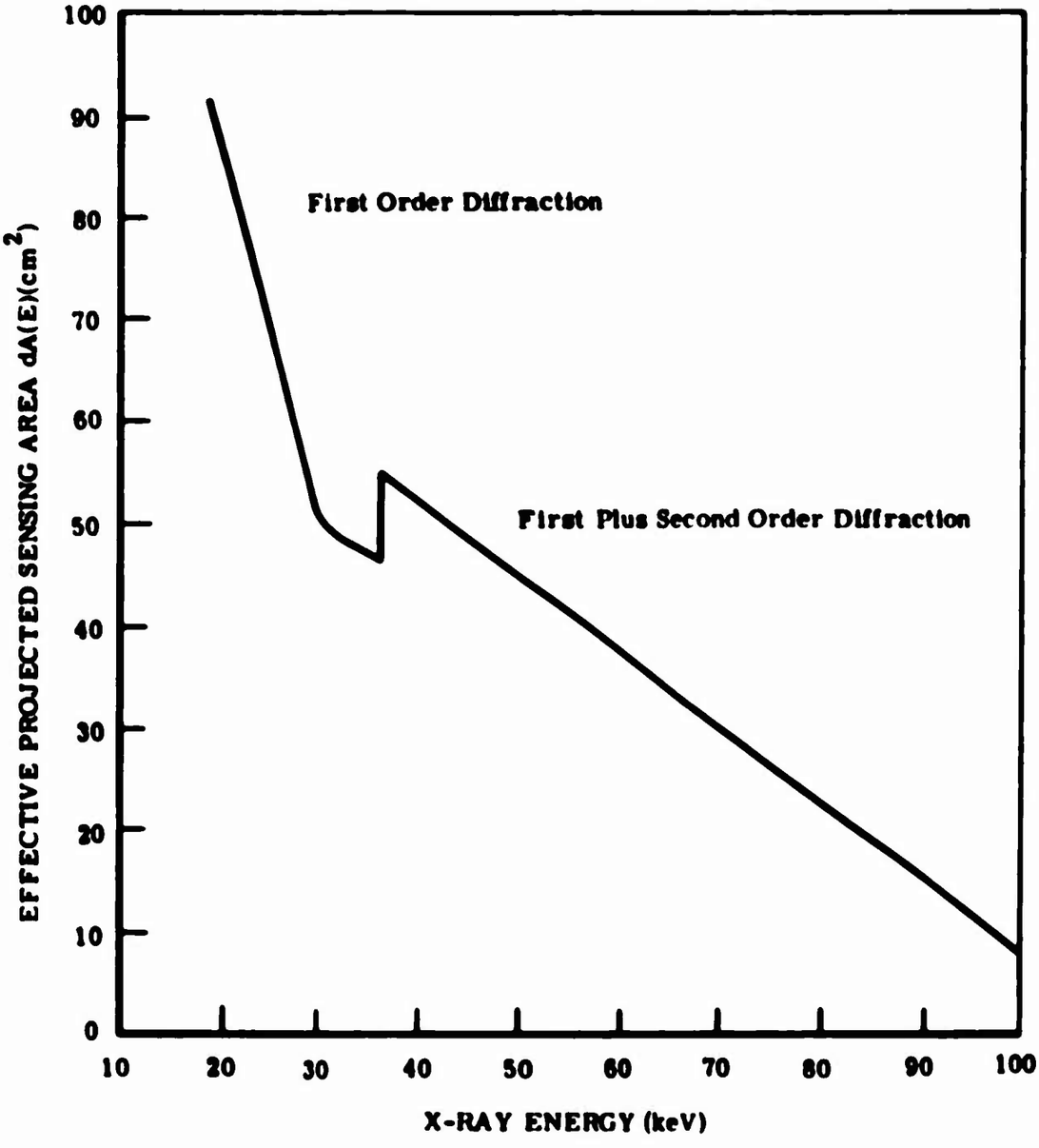

Fig. 16 Variation of effective lens area with energy

with which the LiF crystal planes conform to paraboloids.

Preliminary ray tracing studies have verified the above statements. Using a good approximation of *angular resolution* (through sky scanning techniques) as being one-tenth the *field of view*, we expect an angular resolution of 0.05° or 2-3 arc minutes to be realistic. As with any other optical system, actual measurements of the instrument will be required to know the precise field of view and its angular resolution.

5.2 Minimum Detectable Flux

The ability of any instrument to detect a weak signal is often determined by the noise fluctuations of the background components inherent to the detecting system. In evaluating this noise we note there are three main components to an x-ray background spectrum at 3 g cm^{-2} atmospheric depth:

a) inherent detector background [NaI(Tl)][28] :
4×10^{-4} photons $cm^{-2} sec^{-1} keV^{-1}$

b) diffuse atmospheric radiation [28]
2×10^{-2} photons $cm^{-2} sec^{-1} keV^{-1} sr^{-1}$

and c) diffuse cosmic x-ray flux[29]
2×10^{-2} photons cm^{-2} $sec^{-1} keV^{-1} sr^{-1}$

where all fluxes are centered at 30 keV. Due to the small field of view of the current x-ray telescope ($\pi\theta^2 \simeq 2 \times 10^{-4}$ steradians), the nearly isotropic components (b) and (c) are quite negligible compared to component (a).

Thus, if one considers the energy range 20 to 40 keV, the background counting is 0.04 photons/second. By integrating over the longest practical balloon-observation time, 3600 seconds, there is a total of 150 background photons. Assuming this background obeys a Poisson statistical law, we estimate by a method similar to that outlined by Griesen[30] a minimum detectable signal, $\dot{}_{min}$, at the 99.7% confidence level of $8 \times 10^{-6} cm^{-2} sec^{-1} keV^{-1}$ centered at 30 keV. This is equivalent to 2×10^{-3} of the Crab Nebula. The sensitivity decreases at higher energies due to the decreasing diameter of diffracting annuli. This is at least 2½ times more sensitive than some alternate techniques[31,32].

The combination of broad energy coverage, small field of view, and high flux sensitivity make this instrument capable of a number of significant astronomical observations:

a) measurement of celestial source spectra using an energy sensitive detector;

b) detection of weak x-ray sources;

c) measurement of time-varying x-ray sources; non-periodic and periodic (pulsars);

d) polarimetry of x-ray sources using a Thomson scattering detector such as that of Angel et al[8].

6.0 DISCUSSION

Celestial x-ray concentrating devices using the x-ray diffraction principle are competitive with (or exceed) existing techniques of x-ray astronomy. The minimum detectable flux (8×10^{-6} photons cm^{-2} sec^{-1} keV^{-1}) of the Confocal Paraboloid X-ray Lens significantly exceeds the limit of any existing system. The Asymmetric Bragg Cone surfaced with an efficiently diffracting crystal such as graphite may be useful as a self-concentrator; however, it is definitely a competitive x-ray polarimeter. The cone geometry presented herein considers only the case of parallel incident x-rays; the geometry may be adapted to converging or diverging incident beams as would be necessary to utilize the polarimeter near the focus of a grazing incidence x-ray telescope.

The energy range of applicability of a diffraction-based system is determined only by the crystals available. Crystals are known which would extend the range to both higher and lower energies; e.g., utilization of "layered soap film crystal" would extend the range of the confocal paraboloid instrument well into low energies (0.5 keV).

The experimental diffraction data for LiF prove false the old rule that a Bragg crystal must be 1/μ thick for optimum diffracted intensity; much thinner crystals diffract most efficiently. This happy circumstance together with crystal surface preparation to obtain high diffracted intensity make the Bragg geometry most attractive for light weight, sensitive astronomical instruments.

For the two instruments described herein the integrated reflection coefficient, R, was used to calculate the effective gain. To state a general rule: The effective gain is equal to the product of the incremental diffracting area and the integrated reflection coefficient. This principle may be used to determine (or predict) the gain of any diffraction-based instrument.

7.0 REFERENCES

1. H. Wolter, Ann. Physik 10, 94 (1952); ibid., p. 286.
2. R. Giacconi, Scientific American 217, 36 (1967).
3. F. W. Kantor, Trans. N.Y. Acad. Sci. 30, 1100 (1968).
4. T. R. Lindquist, W. R. Webber, Can. J. Phys. 46, S1103 (1968).
5. F. W. Lytle, "A Focusing X-ray Telescope Using Asymmetric Bragg Reflection", presented at Pittsburgh Diffraction Conference, 1 Nov. 1967, Pittsburgh, Pa. (unpublished)
6. F. W. Lytle and R. G. Bingham, "X-ray Telescope Using Asymmetric Bragg Crystal-Plane Diffraction", Boeing Document D1-82-0720, May 1968.
7. R. G. Bingham, F. W. Lytle, C. D. Clark, "Cosmic X-ray Polarimeter", Bull. Am. Phys. Soc. 13, 1412 Nov. (1968). Presented at Fall Meeting APS.
8. J. R. P. Angel, R. Novick, P. VandenBout, and R. Wolff, Phys. Rev. Let. 22, 861 (1969).
9. A. A. Sanin, A. U. Zharko, A. G. Nikolaev, and A. S. Melioranskii, Instr. and Exp. Tech. No. 1, 62 (Jan-Feb 1968).
10. R. W. James, "The Optical Principles of the Diffraction of X-rays", (G. Bell and Sons, London, 1950) p. 45.
11. Ibid., p. 269
12. S. Chandrasekhar, Adv. in Physics 9, 363 (1960).
13. D. A. Lind, W. J. West, J.W.M. DuMond, Phys. Rev. 77, 475 (1950).

14. B. W. Batterman, H. Cole, Rev. Mod. Phys. 36, 681 (1964).

15. F. W. Lytle, Science (to be published).

16. J. Vierling, J. V. Gilfrich, L. S. Birks, Applied Spectroscopy (to be published).

17. Union Carbide Corp., Parma, Ohio. Special thanks for loaning samples for these measurements.

18. R. W. Gould, S. R. Bates, and C. J. Sparks, Appl. Spectroscopy 22, 549 (1968).

19. L. D. Jennings, Acta Cryst. A24, 472 (1968).

20. S. Miyake, S. Togawa, S. Hosoya, Acta Cryst. 17, 1083 (1964).

21. P. Suortti and T. Paakkari, J. Appl. Cryst. 1, 121 (1968).

22. H. Cole, F. W. Chambers, C. G. Wood, J. Appl. Phy. 32, 1942 (1961).

23. S. Chandrasekhar, S. Ramaseshan, and A. K. Singh, Acta Cryst. A25, 140 (1969).

24. M. Renninger, Z. Krist. 97, 95 (1937).

25. M. Renninger, Adv. X-ray Anal. Vol. 10, Newkirk and Mallett, Ed. Plenum Press, New York 1967, pp. 32-41.

26. P. B. Hirsch and G. N. Ramachandran, Acta Cryst. 3, 187 (1950).
P. Gay, P. B. Hirsch and J. N. Kellar, Acta Cryst. 5, 7 (1952).
R. C. Evans, P. B. Hirsch, and J. N. Kellar, Acta Cryst. 1, 124 (1948).

27. R. W. James, op. cit. pp. 54 and 167.

28. L. F. Peterson, A. S. Jacobson, R. M. Pelling and D. A. Schwartz, Can. J. Phys. 46, S437 (1968).

29. J.A.M. Bleeker, et. al., Can. J. Phys. 46, S461 (1968).

30. K. Greisen, *Perspectives in Modern Physics* (R. E. Marshak, ed.), John Wiley and Sons, Inc., New York, 377, 1966.

31. I. S. Glass, Mass. Inst. of Tech., CSR Report, No. P-68-5, 1968.

32. R. C. Haynes, D. V. Ellis, G. J. Fishman, S. W. Glenn and J. D. Kurfess, Ap. J. 155, L31-L34, 1969.

8.0 ACKNOWLEDGMENTS

We thank C. D. Clark and D. E. Sayers for many calculations, measurements and profitable discussions and P. W. Olson, machinist extraordinary.